energies

MDPI

Article

Cooling Performance Optimization of Direct Dry Cooling System Based on Partition Adjustment of Axial Flow Fans

Wenhui Huang [1,2], Lei Chen [1,2], Weijia Wang [1,2], Lijun Yang [1,2,*] and Xiaoze Du [1,2]

[1] Key Laboratory of Condition Monitoring and Control for Power Plant Equipment, Ministry of Education, Beijing 102206, China; hwh@ncepu.edu.cn (W.H.); chenl@ncepu.edu.cn (L.C.); wangwj@ncepu.edu.cn (W.W.); duxz@ncepu.edu.cn (X.D.)

[2] School of Energy Power and Mechanical Engineering, North China Electric Power University, Beijing 102206, China

* Correspondence: yanglj@ncepu.edu.cn; Tel.: +86-10-61773373; Fax: +86-106-177-3877

Received: 2 May 2020; Accepted: 14 June 2020; Published: 19 June 2020

Abstract: Axial flow fans play key roles in the thermo-flow performance of direct dry cooling system under windy conditions, so the energy efficiency of a power generating unit can be improved by optimizing the operation strategies of the axial flow fans. In this work, various measures based on the partition adjustment of axial flow fans with constant power consumption of a 2 × 660 MW power plant are studied by computational fluid dynamics (CFD) methods. The results show that increasing the rotational speed of the windward fans is beneficial to reduce the inlet air temperature and increase the mass flow rates of the fans, which enhance the heat rejections of the air-cooled condensers, especially at high wind speeds. Moreover, the turbine back pressures for the optimal and original cases are achieved by iterative methods, with the largest drop of 2.77 kPa at the wind speed of 12 m/s for 110-case 3 in the wind direction of −90°. It is recommended to adopt 110-case 1 and 110-case 3 at low and high wind speeds, respectively, in the wind directions of 90° and −90°, while 110-case 2 is always the best choice in the 0° wind direction.

Keywords: direct dry cooling system; air-cooled condenser; axial flow fan; partition adjustment; cooling performance; turbine back pressure

1. Introduction

The water consumption in traditional power plants is considerable, especially during the process of exhaust steam cooling by circulating water, which causes environmental issues simultaneously [1]. The direct dry cooling system (DDCS) has been widely applied in arid regions due to its excellent water-saving characteristics [2]. It adopts large axial flow fans to force cooling air to flow through finned tube bundles, taking away the heat rejection from exhausted steam, so the cooling capacity of DDCS depends largely on the working conditions of axial flow fans.

As is well known, the cooling performance of DDCS is highly susceptible to environmental conditions, such as the ambient temperature and crosswind, among others. Yang et al. [3,4] studied the effects of crosswind on the thermo-flow characteristics of DDCS numerically and concluded that the performance deterioration of windward fans with higher inlet air temperatures and lower air flow rates results in the bad cooling performance of the condenser cells. However, the performance is recovered for the condenser cells along the wind direction. Rooyen et al. [5] found that the flow distortions and low-pressure region caused by the crosswind affects the heat rejection of the upwind condenser cells. Wang et al. [6] investigated the influence of buildings around the air-cooled condensers (ACCs) in different wind directions. Liu et al. [7] found that the hot air recirculation is greatly affected by the wind direction and wind speed. Gu et al. [8,9] proposed the wind tunnel test as an effective way to study the impacts of ambient wind for the design of power plants.

For restraining the impact of ambient winds, many measures have been proposed, including various deflectors [10–13], water spray cooling methods [14,15] and new layouts [16–18]. Moreover, the cooling air is driven by axial flow fans, so the operating conditions of the axial flow fans are of great concern for the cooling performance of DDCS. Duvenhage et al. [19,20] and Meyer [21] pointed out that crosswind causes flow separation and results in the reduced flow rates of fans, especially for the windward ones. Hotchkiss et al. [22] numerically and experimentally studied the influence of off-axis inflow on the performance of axial flow fans. In the existing direct dry cooling power plant, it is a more economical and feasible measure to optimize the operation of fans for improving the cooling performance of the air-cooled condensers. He et al. [23] explored the effects of the installation angle of fans, and found that the regulation strategies can increase the net power output of a power plant, while the adjustment of the leeward fans has nothing to do with the performance of DDCS. Moreover, the increased rotating speed of windward axial flow fans is beneficial to the performance of ACCs and the net power output [24]. Furthermore, the regulation of the entire fan array is recommended to improve the energy efficiency of a power plant [25]. Yang et al. [26] proposed the closed-loop control of the fan speed to reduce coal consumption while improving the load response speed for a power plant.

The aforementioned researches show that crosswind results in the poor performance of DDCS, but the majority of the improvement measures are focused only on the operation of peripheral fans or based on integrated modifications so-called "try and error". In fact, the first few rows of upwind fans are most affected by ambient wind. On account of these issues, this work proposed a new control strategy with changing the rotational speeds of windward fans to relieve adverse wind effects. The fan array is divided into the windward block and leeward block and the rotational speeds of fans in the two blocks are adjusted simultaneously to keep the total power consumption of fans constant. The thermo-flow performances of DDCS are solved by CFD methods, by which axial flow fans optimizations at various wind conditions (e.g., wind speed and wind direction) are obtained, so that the energy efficiency of a power generating unit gets improved, which can contribute to the optimal operation of a power generating unit.

2. Models and Approaches

2.1. Physical Models

A typical 2 × 660 MW direct dry cooling power plant mainly includes boilers, steam turbines, air-cooled condensers and a chimney, with the detailed layout shown in Figure 1a. The two boilers share one chimney, which are next to the turbines, and the air-cooled condensers are located on the other side of the turbines with tens of reinforced concrete cylinders supported. For each condenser, it consists of 56 cells arranged in a 7 × 8 array. Therefore, the total number of 112 (7 × 16) condenser cells is considered, with 7 condenser cells in each column sharing one steam duct. Three wind directions are specified, 90° (-y direction), 0° (-x direction) and −90° (y direction). Figure 1b schematically shows the structures of an air-cooled condenser cell and flat-finned tube bundles, and the specific parameters of the fan and finned tube bundles are the same as those in [27], with the values listed in Table 1.

As is known in previous research, the first few rows of windward condenser cells are affected seriously by ambient wind and the air flow rates of fans get drastically reduced. For improving the performance of axial flow fans in the presence of winds, the thermo-flow characteristics of DDCS are investigated by adjusting the rotational speed of the windward fans while keeping the total power consumption of fans constant in this work. As shown Figure 2a–i, all of the cooling fans are divided into two parts, the windward fans and the other fans. Three different methods are proposed to partition: the first row on the windward side and the others (case 1); the first two rows and the others (case 2); and the first three rows and the others (case 3). The rotational speed of fans in the windward block is adjusted to 90% n_0, 95% n_0, 105% n_0 and 110% n_0, respectively, and the other fans also make corresponding adjustments. Each strategy is named according to the adjustment method, that is, the case for adjusting the rotational speed of fans in the first windward row to 90% n_0 is named 90-case 1, and so on.

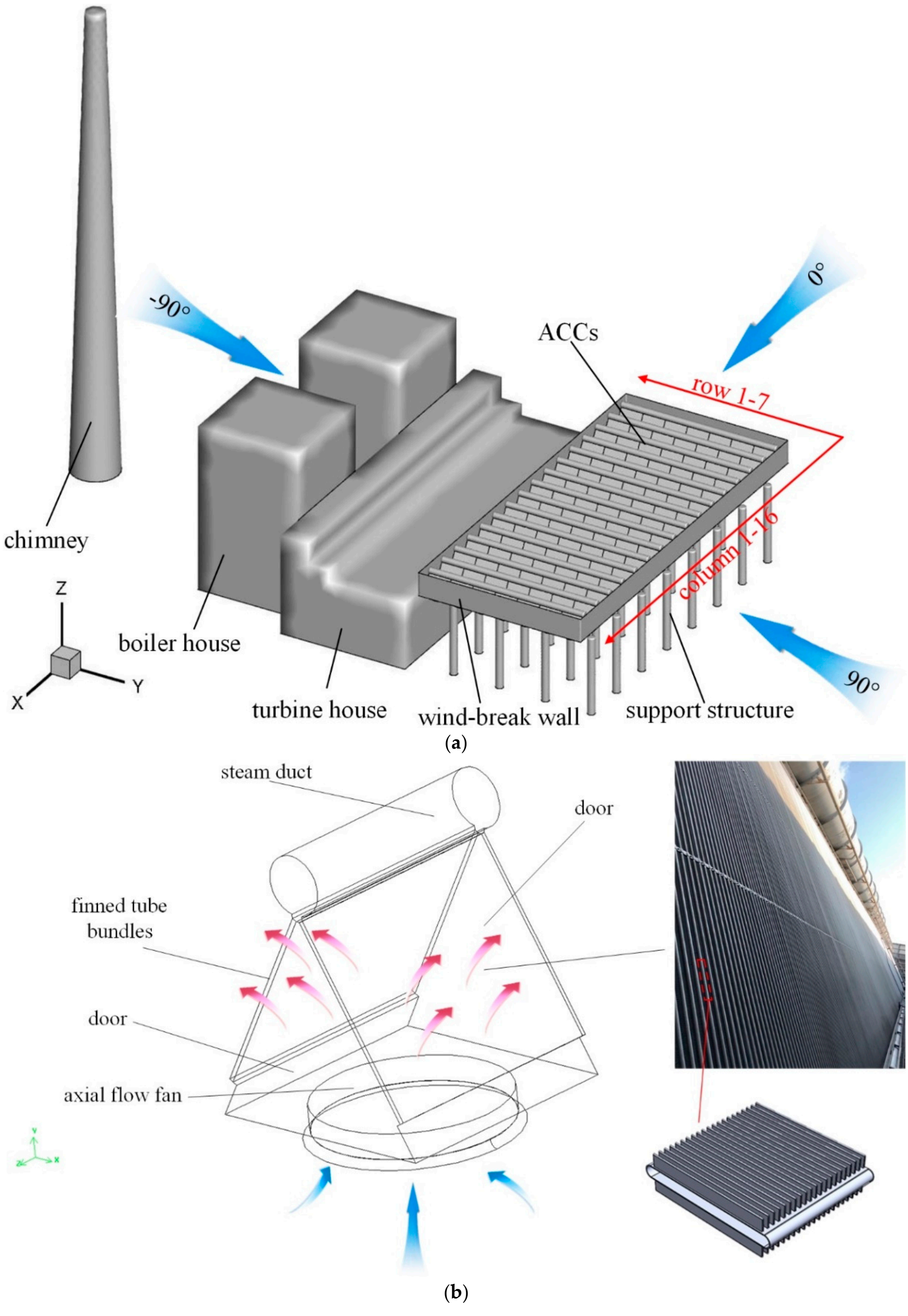

Figure 1. Schematics of the representative 2 × 660 MW direct dry cooling power plant. (**a**) ACCs, main buildings and wind directions; (**b**) condenser cell and flat-finned tube bundles.

Table 1. Geometric parameters of ACCs.

Parameter	Value
Diameter of axial flow fan (m)	9.144
Apex angle of finned flat tube bundles (°)	59.4
Major axis of base tube (m)	0.219
Short axis of base tube (m)	0.019
Length of fin (m)	0.2
Height of fin (m)	0.019
Thickness of fin (m)	0.00025
Pitch of fin (m)	0.0023
Height of ACC platform (m)	45

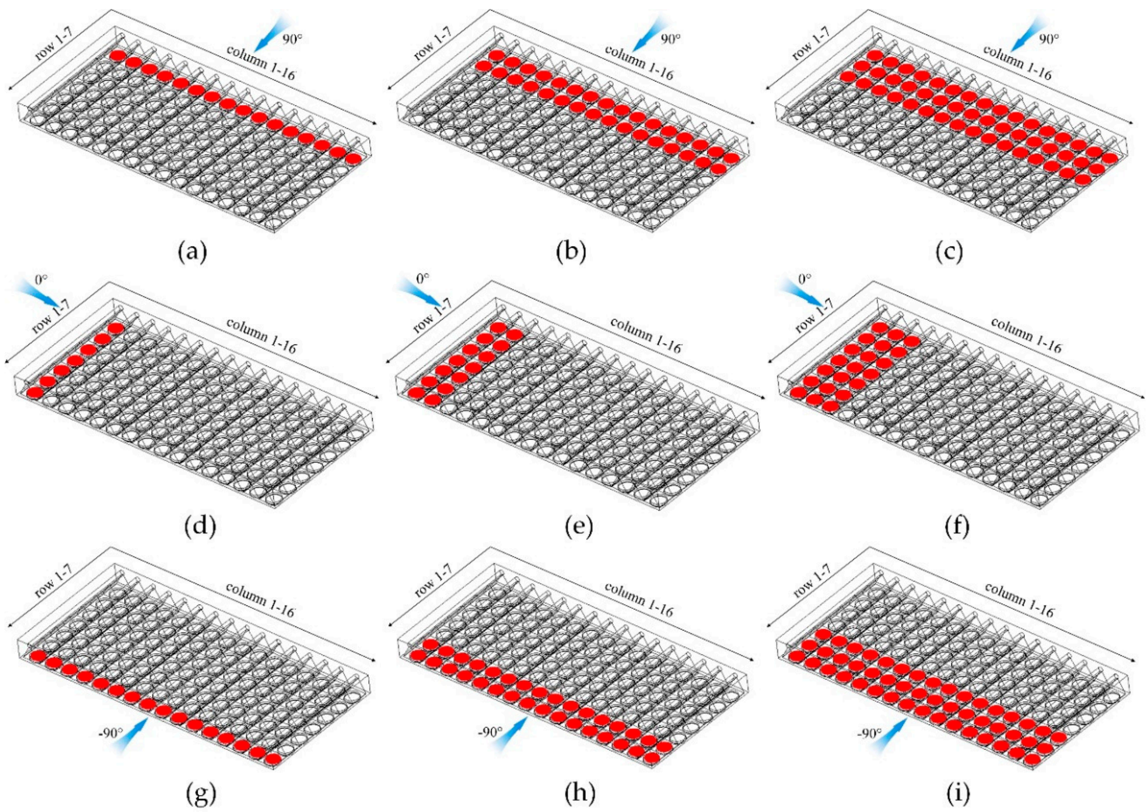

Figure 2. Schematics of the partition methods. (**a**) Case 1 in 90° wind direction; (**b**) case 2 in 90° wind direction; (**c**) case 3 in 90° wind direction; (**d**) case 1 in 0° wind direction; (**e**) case 2 in 0° wind direction; (**f**) case 3 in 0° wind direction; (**g**) case 1 in −90° wind direction; (**h**) case 2 in −90° wind direction; (**i**) case 3 in −90° wind direction.

2.2. Mathematical Models and Methods

The air-side flow and heat transfer of DDCS follow the conservation equations of mass, momentum, energy and turbulence, which can all be described by the following generic form [28].

$$\nabla \cdot \left(\rho \vec{u} \varphi - \Gamma_\varphi \nabla \varphi\right) = S_\varphi + S'_\varphi, \tag{1}$$

where ρ is the air density, φ is the dependent variable, Γ_φ is the coefficient of diffusion. S_φ represents the source term of variable φ, and $S_\varphi{}'$ is the additional source term and set at zero except for the finned tube bundles zone. The momentum and energy equations require an additional momentum source term $S_m{}'$ and energy source term $S_e{}'$, respectively, in the finned tube bundles zone, with the following expressions [16].

$$S'_m = -\frac{\Delta p_j}{L_j}, \tag{2}$$

$$S'_e = \frac{q_j}{L_j}, \tag{3}$$

where Δp_j, q_j and L_j are the pressure drop, heat flux and the thickness of finned tube bundles in the j direction, respectively. For the turbulence simulation, the realizable k-ε model is adopted because of its excellent performance in the prediction of vortices, rotation and separated flows.

The finned tube bundles of ACCs are treated as radiator surfaces and the pressure drop is an important parameter [29]. By using the method of lumped parameters, the pressure drop Δp of cooling air through the finned tube bundles is assumed to be a proportional function of the air dynamic head, which is shown as follows.

$$\Delta p = k_{\mathrm{L}} \frac{1}{2} \rho u_{\mathrm{f}}^2, \tag{4}$$

where u_{f} is the face velocity normal to the radiator surface and k_{L} represents the non-dimensional loss coefficient with the following polynomial form.

$$k_{\mathrm{L}} = \sum_{\mathrm{n}=1}^{\mathrm{N}} r_{\mathrm{n}} u_{\mathrm{f}}^{\mathrm{n}-1}, \tag{5}$$

where N is set to 5 and r_{n} refers to the polynomial coefficient with the value in Reference [4].

According to Newton's law of cooling, the heat flux q between the cooling air and steam can be calculated as follows.

$$q = h(t_{\mathrm{wall}} - t_{\mathrm{a}}) = h'(t_{\mathrm{wall}} - t_{\mathrm{a2}}) = h'(t_{\mathrm{s}} - t_{\mathrm{a2}}), \tag{6}$$

where h is the convection heat transfer coefficient, t_{wall} is the temperature of the finned tube wall, t_{a} is the mean temperature of the cooling air, and t_{a2} is the outlet air temperature of the radiator while t_{s} is the temperature of the exhaust steam. It can be considered that t_{wall} and t_{s} are equal when the thermal resistance of the condensation and wall conduction is ignored. h' is the empirical convective heat transfer coefficient of the radiator model with the following expression.

$$h' = \sum_{\mathrm{n}=1}^{\mathrm{N}} h_{\mathrm{n}} u_{\mathrm{f}}^{\mathrm{n}-1}, \tag{7}$$

where N is set to 3 and h_{n} is the polynomial factor obtained by heat transfer experiments as h_1 = 3015.5, h_2 = 386.27, h_3 = −11.976. The heat transfer experiments of finned flat tubes are achieved by a wind tunnel test [19], which is considered as a reliable method to obtain the related parameters [30].

The fan model is adopted to simplify the geometry structure of the fan blade, which can be described with two important parameters, the pressure rise Δp and the tangential velocity u_θ. The former is obtained from the performance curve of the typical fan, and the latter is related to the geometry of the real fan and imposed on the fan surface to make the model more accurate, with the following polynomials [31].

$$\Delta p = \sum_{\mathrm{n}=1}^{\mathrm{N}} f_{\mathrm{n}} u_{\mathrm{z}}^{\mathrm{n}-1}, \tag{8}$$

$$u_\theta = \sum_{\mathrm{n}=-1}^{\mathrm{N}} g_{\mathrm{n}} r^{\mathrm{n}}, \tag{9}$$

where N is set to 5, u_{z} is the axial velocity, r is the distance to the fan center, and f_{n} and g_{n} are polynomial coefficients with the same values as Reference [32].

When the operating states of fans change, their characteristic parameters will vary accordingly. For a certain fan, the variations in the parameters obey the similarity principle as follows when only the rotational speed changes [33].

$$\frac{q_{\mathrm{v}}}{q_{\mathrm{v0}}} = \frac{n}{n_0}, \tag{10}$$

$$\frac{p}{p_0} = \left(\frac{n}{n_0}\right)^2, \tag{11}$$

$$\frac{P}{P_0} = \left(\frac{n}{n_0}\right)^3, \tag{12}$$

where n_0 and n are the rated and actual rotational speeds of the fan, q_{v}, p and P are the volumetric flow rate, full pressure and shaft power of the fan at the actual rotational speed, respectively, and q_{v0}, p_0 and P_0 are the corresponding parameters at the rated rotational speed.

In this work, the power consumption of the axial fans is constant. According to Formula (12), the speed of leeward fans is calculated by the following formula when the rotational speed of fans in the windward block is adjusted.

$$\frac{n}{n_0} = \left(\frac{112 - cx^3}{112 - c}\right)^{\frac{1}{3}}, \tag{13}$$

where c is the number of adjusted fans on the windward side and x is the ratio of the actual rotational speed of the upwind fans to the rated rotational speed.

Combining Formulas (8)–(13), the pressure rise and tangential velocity of the fan which deviates from the rated rotational speed can be obtained by the following equations.

$$\Delta p = \sum_{\mathrm{n}=1}^{\mathrm{N}} \left(f_{\mathrm{n}} \left(\frac{n}{n_0}\right)^{3-\mathrm{n}} \right) u_{\mathrm{z}}^{\mathrm{n}-1}, \tag{14}$$

$$u_{\theta} = \sum_{\mathrm{n}=-1}^{\mathrm{N}} \left(g_{\mathrm{n}} \left(\frac{n}{n_0}\right) \right) r^{\mathrm{n}}, \tag{15}$$

At the presence of wind, the wind speed u_{z} is imposed on the inlet surface of the computational domain by using a user defined function (UDF), which is calculated by the following power-law equation [11].

$$u_{\mathrm{z}} = u_{\mathrm{w}} \left(\frac{H}{10}\right)^{0.2}, \tag{16}$$

where u_{w} is the wind speed at the height of 10 m, which is considered as the reference speed, and H is the height from the ground.

The boundary conditions are shown in Figure 3, with the wind direction of 90° as an example. The windward surface is set as the velocity inlet and the opposite surface is the outflow. Both sides and top surfaces are considered to be symmetry. The ground is specified as the non-slip and adiabatic wall and the standard wall functions are adopted. The boundary conditions for the other two wind directions are similar. The operating temperature is 290.15 K. The computational domain is a 2400 × 2400 × 720 m cube, which is large enough to enhance the calculation accuracy and reliability. The details of the boundary conditions are listed in Table 2.

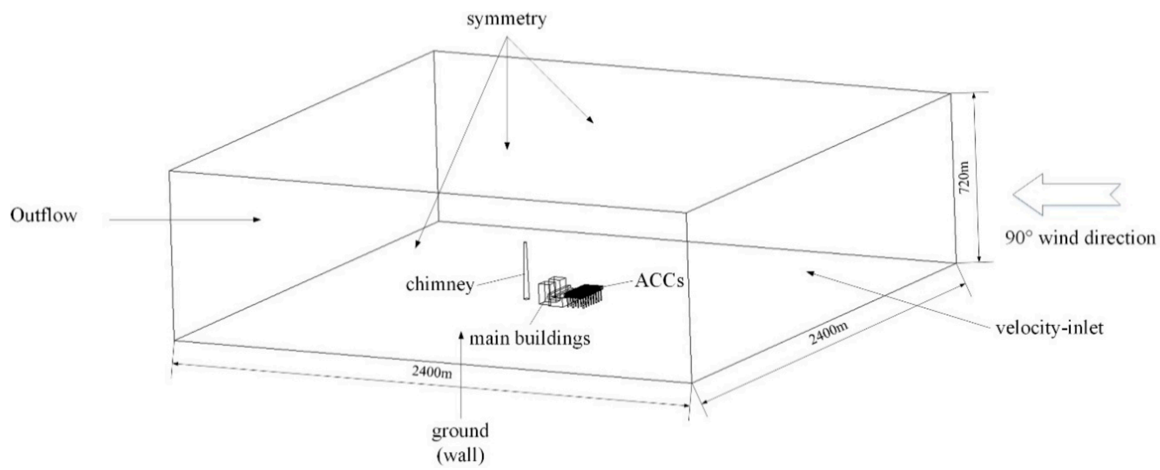

Figure 3. Boundary conditions in the wind direction of 90° and the computational domain.

Table 2. Boundary conditions.

Surface	Wind Condition	Type	Setting
windward surface	with wind	velocity inlet	$u = u_z$, t = 290.15 K
	without wind	pressure inlet	p = 101.325 kPa, t = 290.15 K
leeward surface	with wind	pressure outlet	p = 101.325 kPa, t = 290.15 K
	without wind	pressure inlet	p = 101.325 kPa, t = 290.15 K
side surface	with wind	symmetry	$\partial u/\partial x = 0$, $\partial t/\partial x = 0$ or $\partial u/\partial y = 0$,$\partial t/\partial y = 0$
	without wind	pressure inlet	p = 101.325 kPa, t = 290.15 K
top surface	with wind	symmetry	$\partial u/\partial z = 0$, $\partial t/\partial z = 0$
	without wind	pressure outlet	p = 101.325 kPa, t = 290.15 K
ground		wall	$\partial u/\partial n = 0$, $\partial t/\partial n = 0$
heat exchanger		radiator	$\Delta p = f(u_f)$, $h = f(u_f)$

The CFD software ANSYS FLUENT 16.0 is applied to predict the performance of DDCS in this work. SIMPLE is selected as the pressure–velocity coupling algorithm. The second-order upwind differencing and central differencing schemes are used to discretize the convective and diffusion terms in the governing equations. The divergence-free criteria of scaled residuals for energy and other conservation equations are set as 10-4 and 10-6, respectively. Besides, the air flow rate through the ACCs is also adopted to monitor the reasonable convergence.

2.3. Mesh Independence and Experimental Validation

By the commercial software Gambit, the computational domain is divided into several blocks. The DDCS is located on the central block, so the more adaptive tetrahedral unstructured grids are adopted in this area. Moreover, the sizes of grids for the ACC platform, including fans, radiator surfaces, supported columns and wind-break walls, are set as 0.5 m. For the other surfaces in this block, the grid size is 5 m. The regular hexahedral structured grids are used in other blocks which are all cuboids, and they get sparser when farther away from the center to save computational resources without affecting the accuracy of the calculation.

In order to test the effect of grids on the calculation results, three different grid numbers, 2,310,748, 3,052,216 and 3,855,109, are employed with different grid intervals and named as mesh A, B and C, respectively. The mass flow rates of the axial flow fans are obtained with the wind speeds of 0, 4 and 12 m/s. The contrast results are listed in Table 3, from which can be seen that the differences among the three different grids are small at various wind speeds, especially mesh B and C, so the grid number of 3,052,216 is adopted.

Table 3. The results of the mesh independence test.

Parameter		Mesh A and B (%)	Mesh B and C (%)
Difference in total mass flow rate	0 m/s	2.36	0.22
	4 m/s	3.07	0.29
	12 m/s	4.12	0.38
Maximum mass flow rate difference of single fan	0 m/s	2.95	0.31
	4 m/s	3.52	0.40
	12 m/s	4.71	0.46

By a spot experiment based on a 4 × 600 MW direct dry cooling power plant [11], the inlet air temperature of a certain condenser cell is obtained under the rated load. The model of the power plant was established and a numerical simulation was carried out. The comparison of the experimental and numerical results for the same condenser cell is shown in Figure 4. It can be found that the difference in the inlet air temperature is small enough. Moreover, the experiment of a scaled model of a condenser cell was also made [34], and the comparison with the simulation results shows that the maximum relative error of heat rejections is 10.57% for all cases. The aforementioned comparisons all prove that the computational models and simulation methods, which are adopted in this work, are reliable in predicting the performance of DDCS.

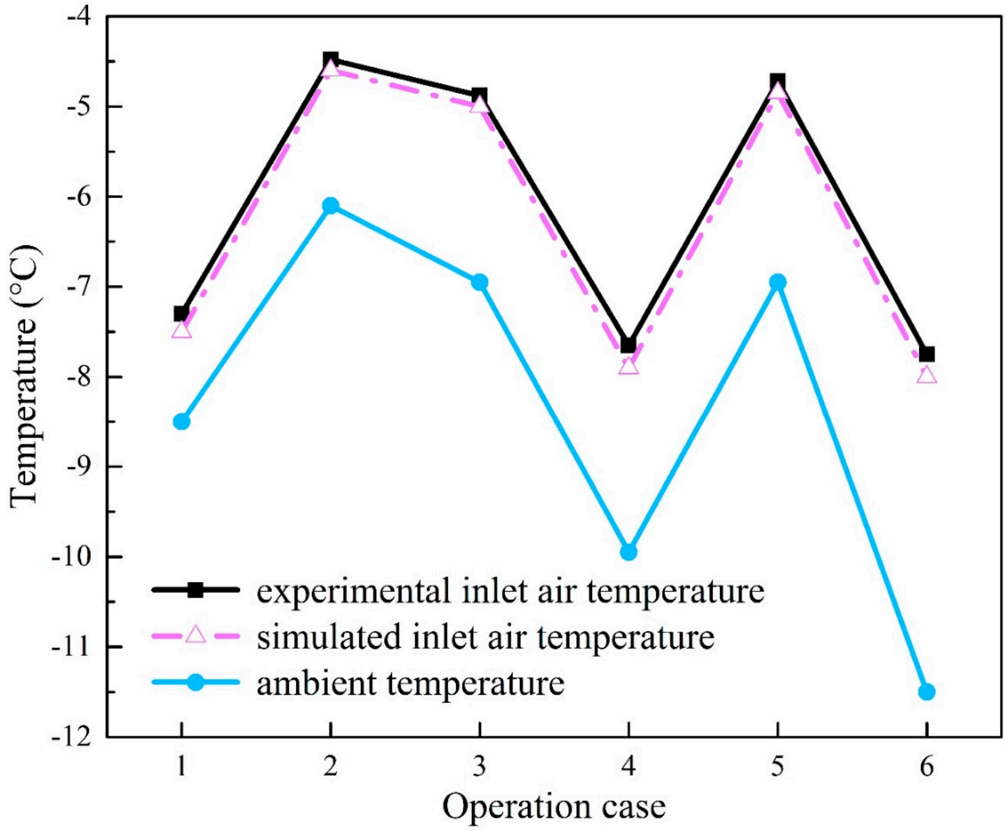

Figure 4. Experimental and computed inlet air temperatures of a specific ACC cell.

3. Results and Discussion

The effects of different strategies on the cooling performance of DDCS under different meteorological conditions are simulated, and the temperature field, mass flow rate, heat rejection, back pressure of turbine, etc., are obtained, by which the optimal strategies for different wind conditions can be proposed.

3.1. Temperature Contour

Figure 5 shows the inlet air temperatures of the axial flow fans in three wind directions at the wind speed of 12 m/s for seven representative cases. When the rotational speed of the windward fans is reduced to 90% n_0, the inlet air temperatures of the first few rows on the windward side are clearly higher than the original case, while the tendency is reversed when the speed of the fans in the windward block increases to 110% n_0. The temperature improvements for 110-case 1 are the most conspicuous in all of the wind directions. Besides, the temperature distributions of the downstream fans are hardly affected, although the rotational speeds are also adjusted. It can be concluded that the inlet air temperatures will be reduced by increasing the rotational speed of the fans on the windward side, which is beneficial to the operation of air-cooled condensers.

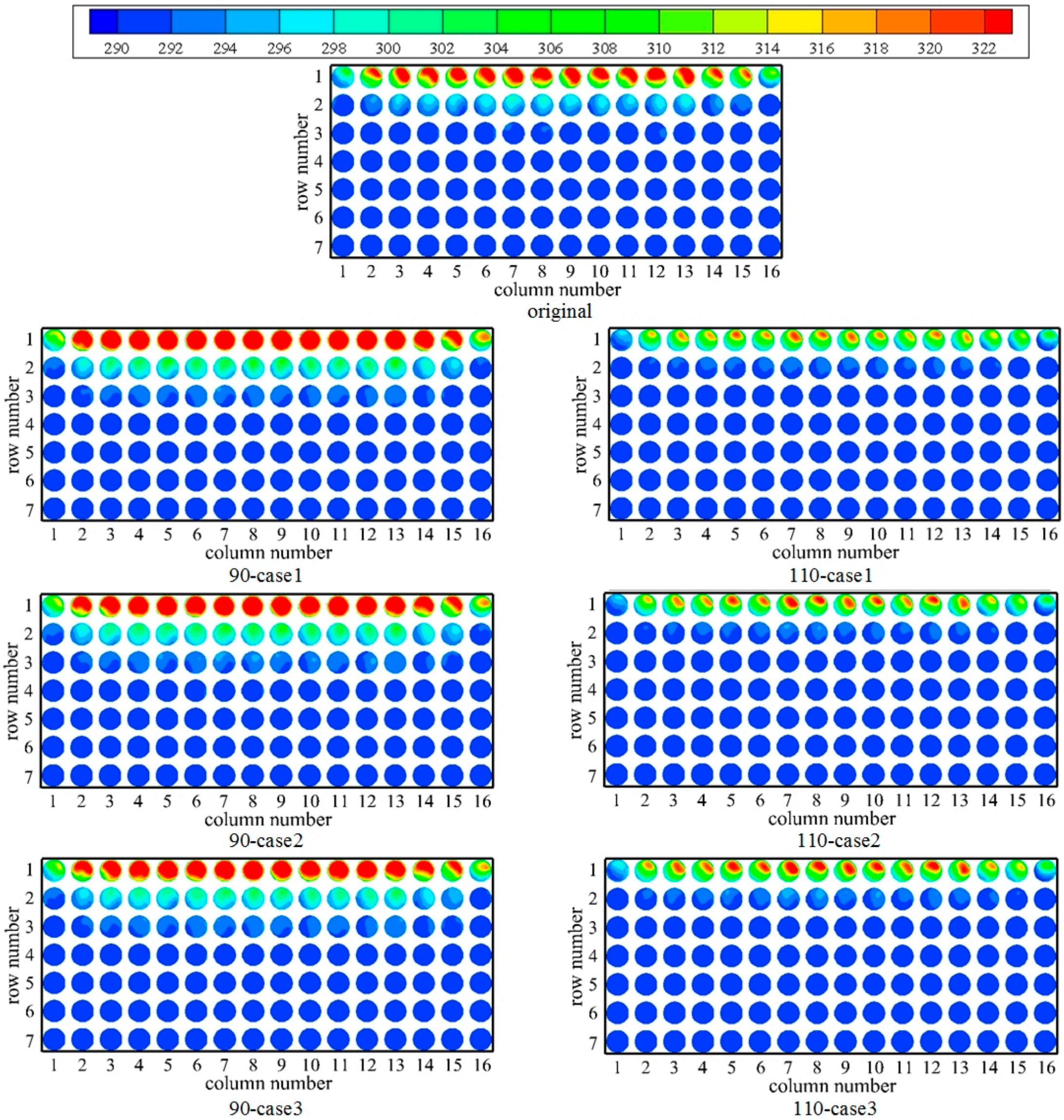

(**a**)

Figure 5. *Cont.*

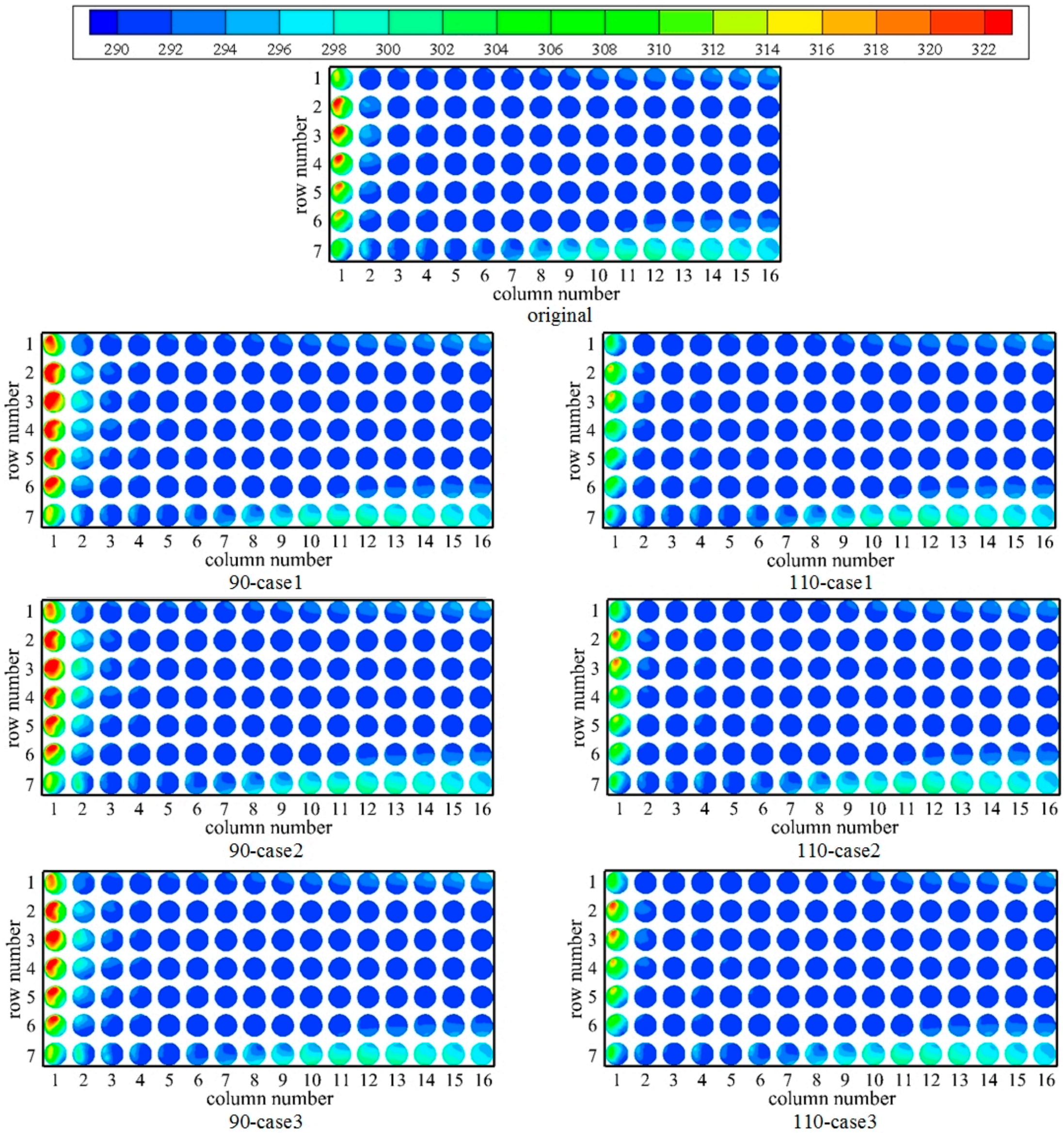

(**b**)

Figure 5. *Cont.*

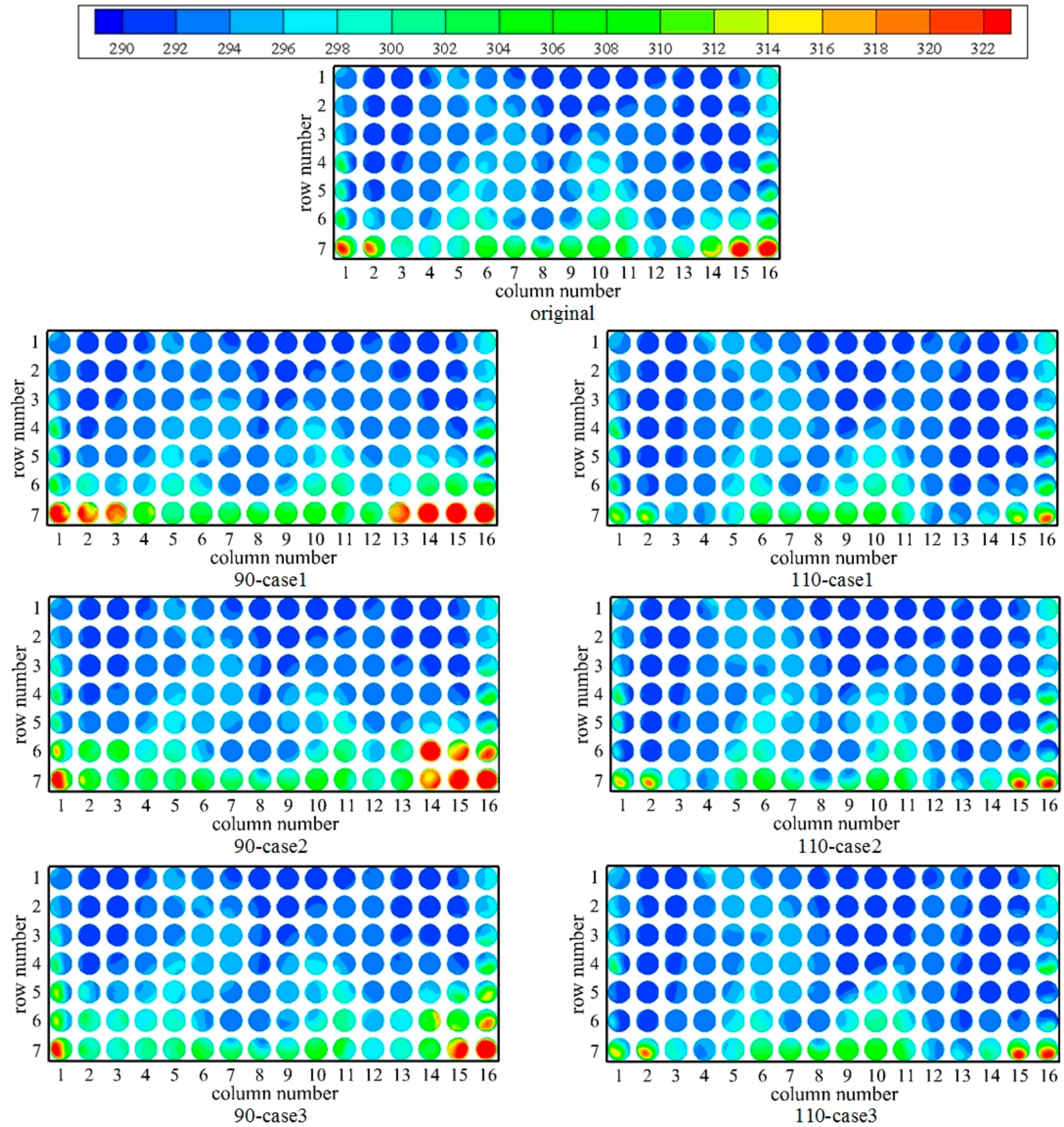

(**c**)

Figure 5. Inlet air temperatures (unit in K) of axial flow fans at the wind speed of 12 m/s. (**a**) In the wind direction of 90°; (**b**) in the wind direction of 0°; (**c**) in the wind direction of −90°.

3.2. Mass Flow Rate of Air

Generally speaking, the mass flow rate of air is positively related to the cooling performance of ACCs. The total mass flow rates of the fans in each row or column along the wind direction are shown in Figure 6. In the wind direction of 90°, the distributions of the mass flow rates of the fans in each column at the wind speed of 3 and 12 m/s are shown in Figure 6a,b, respectively. By increasing the rotational speed of the upwind fans, the air mass flow rates always increase clearly.

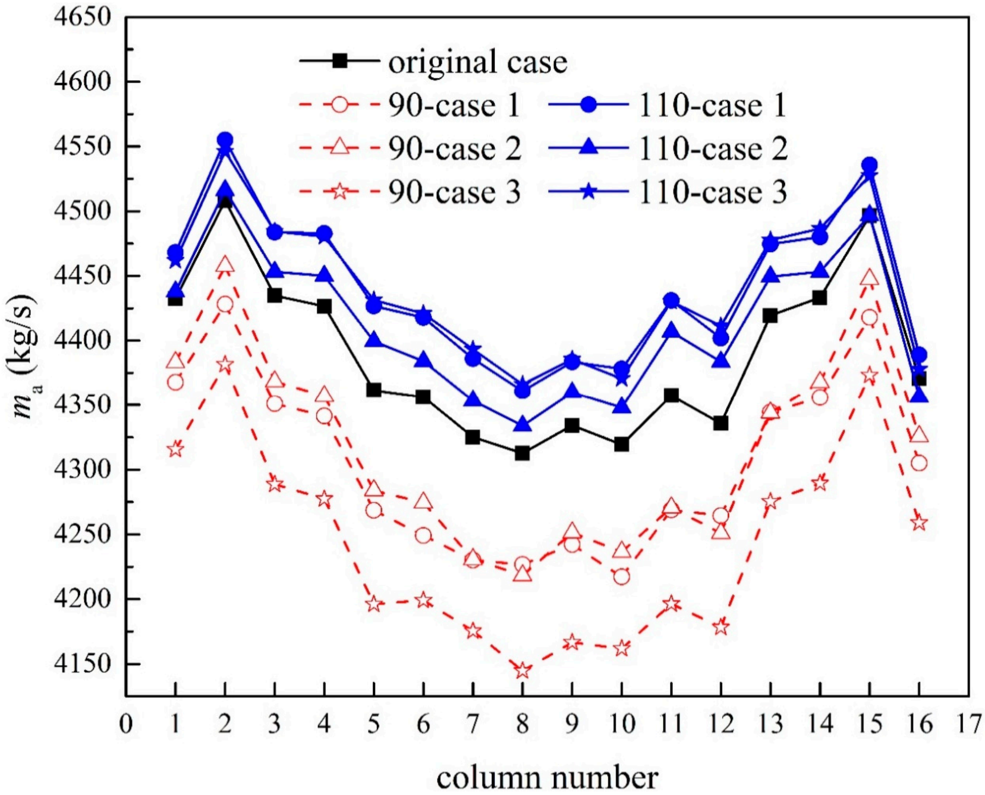

(**a**)

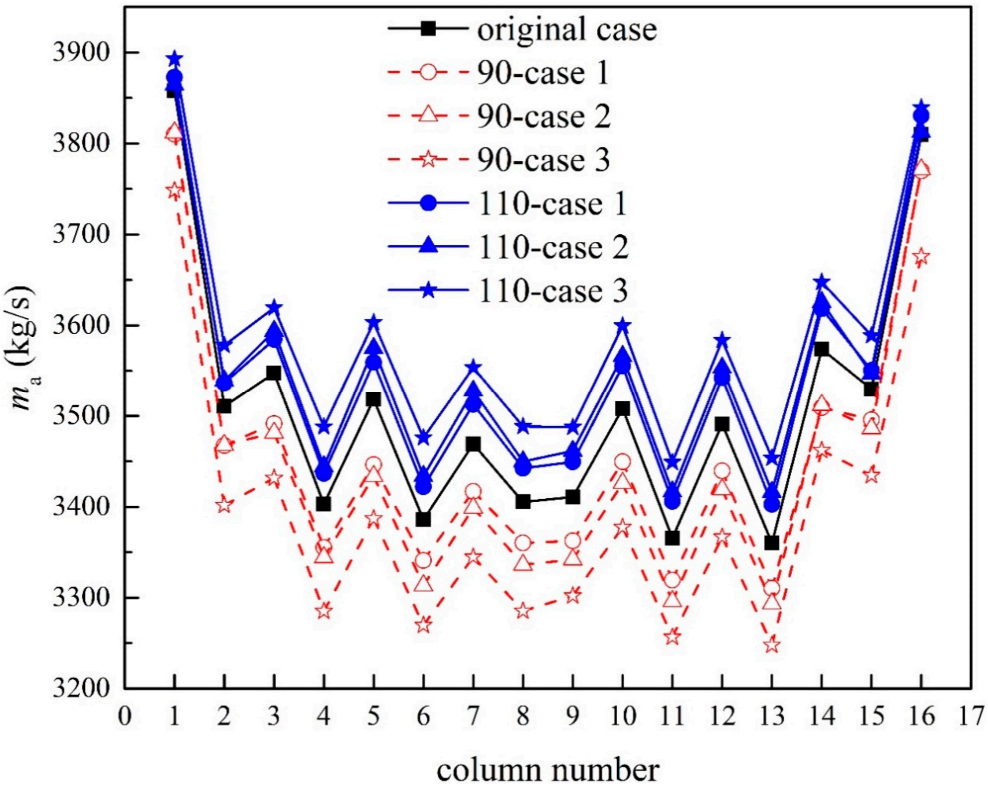

(**b**)

Figure 6. *Cont*.

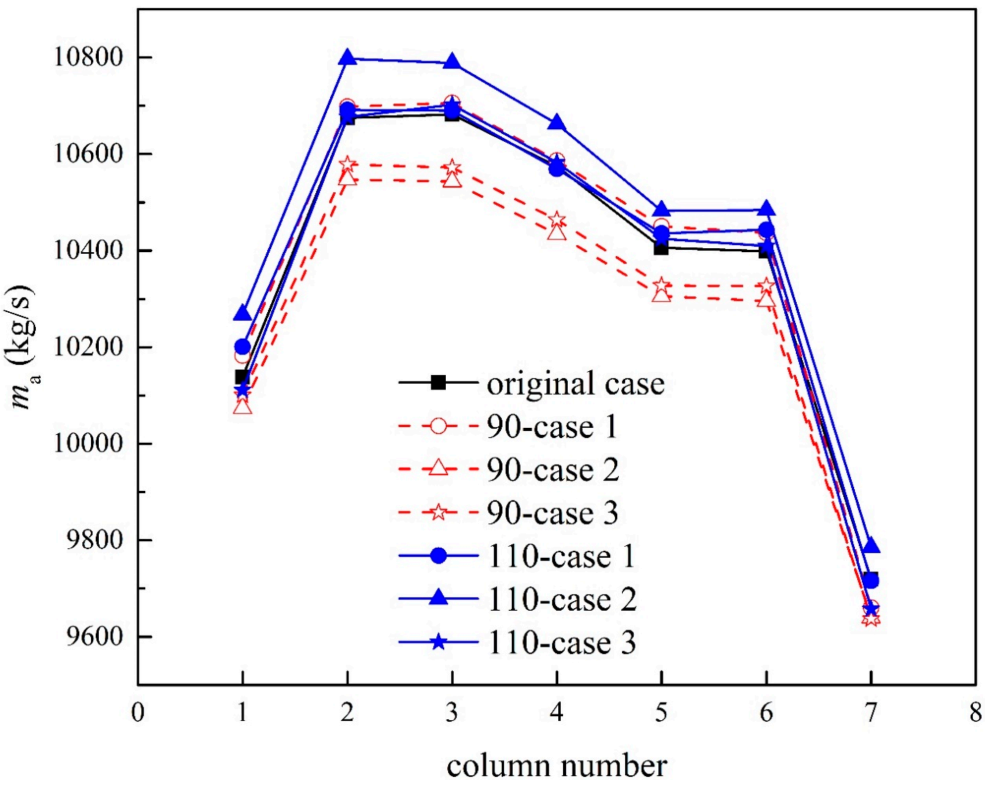

(**c**)

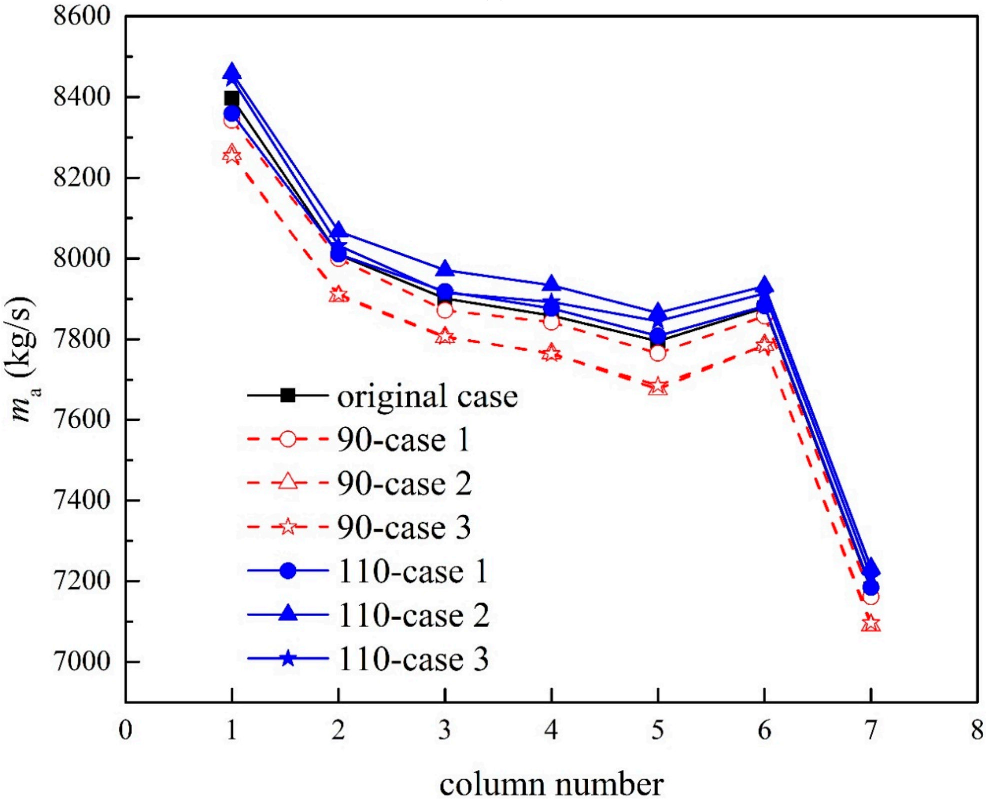

(**d**)

Figure 6. *Cont*.

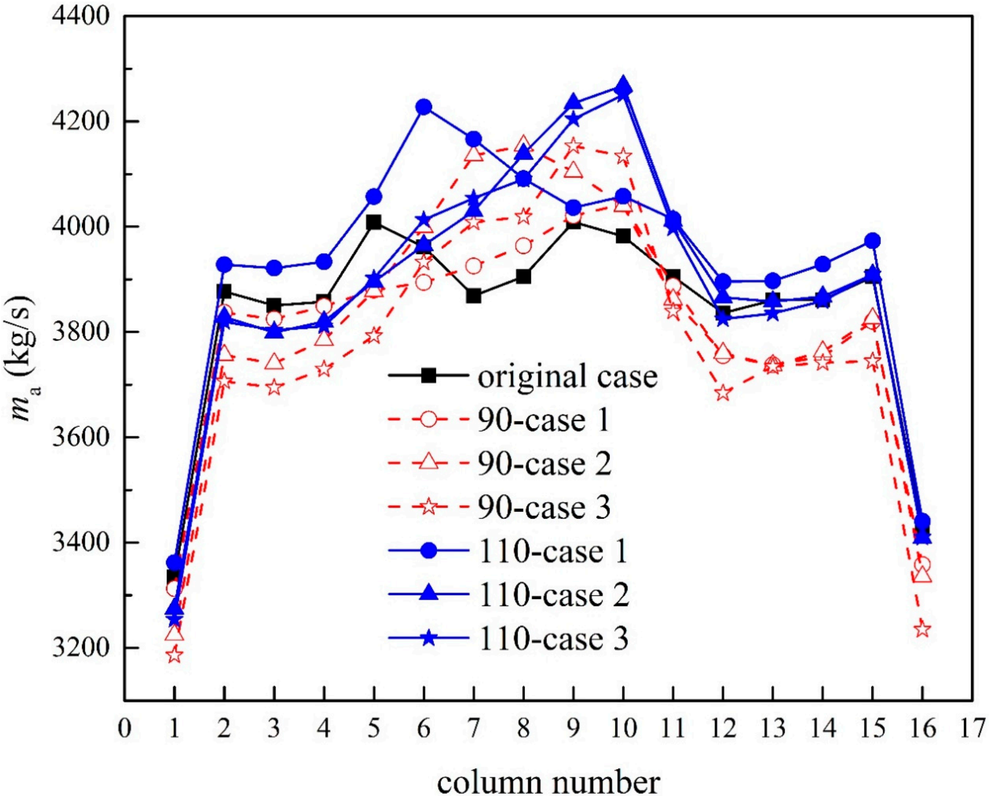

(**e**)

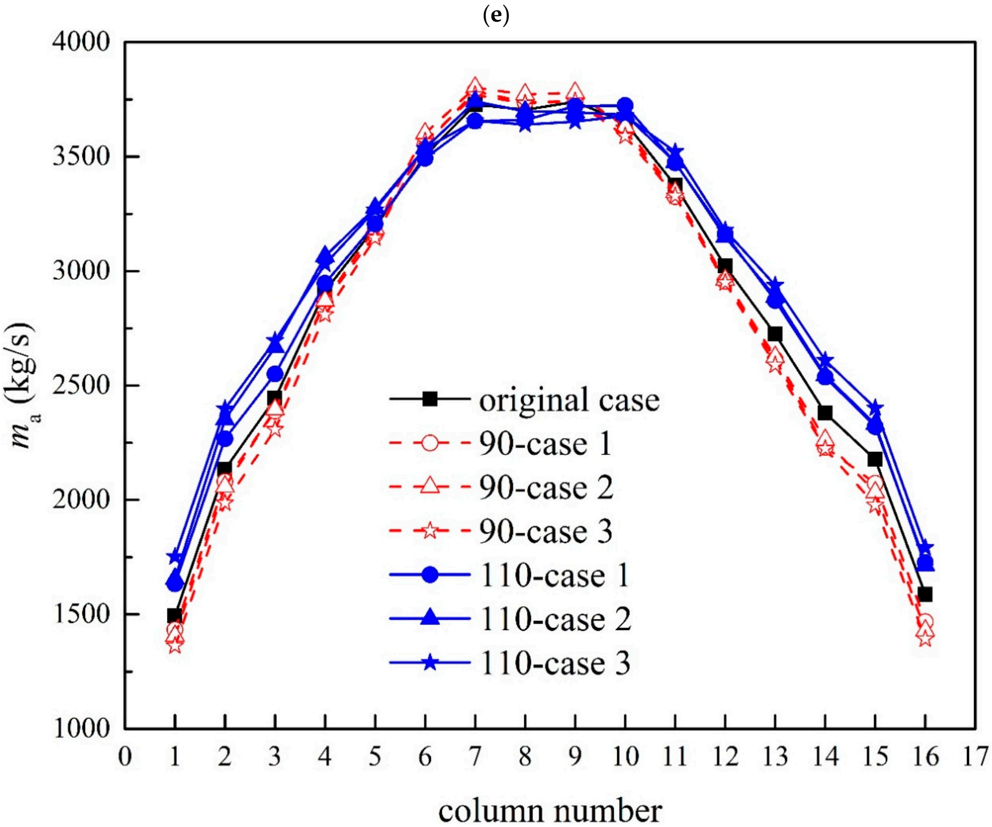

(**f**)

Figure 6. Mass flow rates of various cases. (**a**) Wind speed of 3 m/s and wind direction of 90°; (**b**) wind speed of 12 m/s and wind direction of 90°; (**c**) wind speed of 3 m/s and wind direction of 0°; (**d**) wind speed of 12 m/s and wind direction of 0°; (**e**) wind speed of 3 m/s and wind direction of −90°; (**f**) wind speed of 12 m/s and wind direction of −90°.

At the wind speed of 3 m/s, the mass flow rates of the fans in the 2nd and 15th columns are the highest, while in the middle columns, they are the lowest, which are the combined effects of the hot plume recirculation occurring in the downstream condenser cells of Column 1 and Column 16 and the flow rate reduction in the windward fans with the ambient wind. The mass flow rate distributions of 90-case 1 and 90-case 2 are basically coincidental. 110-case 1 and 110-case 3 have the same situation, while they both perform better than 110-case 2. Moreover, the performance of 90-case 3 is far worse than the other cases.

When the wind speed increases to 12 m/s, as shown in Figure 6b, the mass flow rates of Column 1 and Column 16 are the largest and much higher than the others, because the influence of hot plume recirculation flows on both sides is weak and the reversed air flows on the windward condenser cells are serious at a high wind speed. The results of 90-case 1 and 90-case 2 are relatively close and obviously better than 90-case 3. The improvement of 100-case 3 is biggest, while 100-case 1 and 100-case 2 are almost the same.

Figure 6c,d show the mass flow rate distributions at the wind speed of 3 and 12 m/s, respectively, in the wind direction of 0°. It can be observed in Figure 6c that the flow rates of the Row 1 and Row 7 fans are smaller at the low wind speed because of the hot plume recirculation flows. Due to the main buildings, the flow rates of the fans in Row 7 drop more severely. Specially, the mass flow rates for 90-case 1 slightly increase compared with the original case, while 90-case 2 and 90-case-3 are significantly reduced. On the other hand, the mass flow rates in each row of 110-case 2 are the highest. When the wind speed reaches 12 m/s, the mass flow rates in each row of 90-case 1 are slightly lower than the original case. 90-case 2 and 90-case 3 perform significantly worse. 110-case 1 and 110-case 3 are slightly better than the original case, while the mass flow rates of 110-case 2 are the highest. It can be concluded that 110-case 2 is the best choice in the wind direction of 0° at any wind speed.

The distributions of the mass flow rates in the wind direction of −90° are arched and roughly symmetrical, as shown in Figure 6e,f. At the wind speed of 3 m/s, the mass flow rates of all columns for 110-case 1 increase compared with the original case. For other cases, only the mass flow rates in the middle columns are improved significantly. Besides, the air flow rates on both sides' columns have been greatly reduced for 90-case 1, 90-case 2 and 90-case 3, but are not changed much for 110-case 2 and 110-case 3. At the wind speed of 12 m/s, the mass flow rates for 90-case 1, case 2 and case 3 are increased in the middle columns and reduced in the other columns. However, the situations of 110-case 1, 110-case 2 and 110-case 3 are just opposite. In general, the increases in the total mass flow rates for 110-case 1, 110-case 2 and 110-case 3 are obvious.

3.3. Heat Rejection

The total heat transfer rate of the ACCs can be obtained by CFD simulation according to Equations (6) and (7). In order to compare the difference in heat rejection among the various cases, a dimensionless coefficient ε_Q is proposed to represent the improvement in the heat rejection with the following form.

$$\varepsilon_Q = \frac{Q - Q_0}{Q_0}, \tag{17}$$

where Q and Q_0 stand for the heat rejections of the proposed case and original case under the same environmental conditions, respectively.

Figure 7 gives the ε_Q for all cases under the same windy condition. In Figure 7a, the improvement in heat rejection in the wind direction of 90° at various wind speeds is presented. Generally speaking, the heat rejection gets larger as the rotational speed of the fans in the windward block increases by using the same partition method. The heat rejection for 110-case 1 is largest at the wind speed of 3 m/s, and 110-case 3 performs best when the wind speed is greater than 6 m/s. Moreover, the largest improvement in heat rejection at the wind speed of 3 m/s is only 1.18%. When the wind speed is higher than 3 m/s, the ε_Q is close to 3%.

The results in the wind direction of 0° are shown in Figure 7b. The heat rejections for 110-case 2 are the largest at various wind speeds. Moreover, it is always beneficial to increase the rotational speed of upwind fans except 105-case 1. The improvements of heat rejection are much smaller in this wind direction.

In the wind direction of −90°, the heat rejections for 110-case 1 are the largest at the wind speeds of 3 and 6 m/s, especially at the low wind speed, as shown in Figure 7c. When the wind speed reaches 9 m/s, the improvements in heat rejection for 110-case 3 are largest and increase with increasing the wind speed. The largest value of ε_Q arrives at 4.02% at the wind speed of 12 m/s, which is also the maximum in all wind directions.

The detailed mass flow rate and heat rejection of DDCS for the proposed strategies and original cases are listed in Table 4.

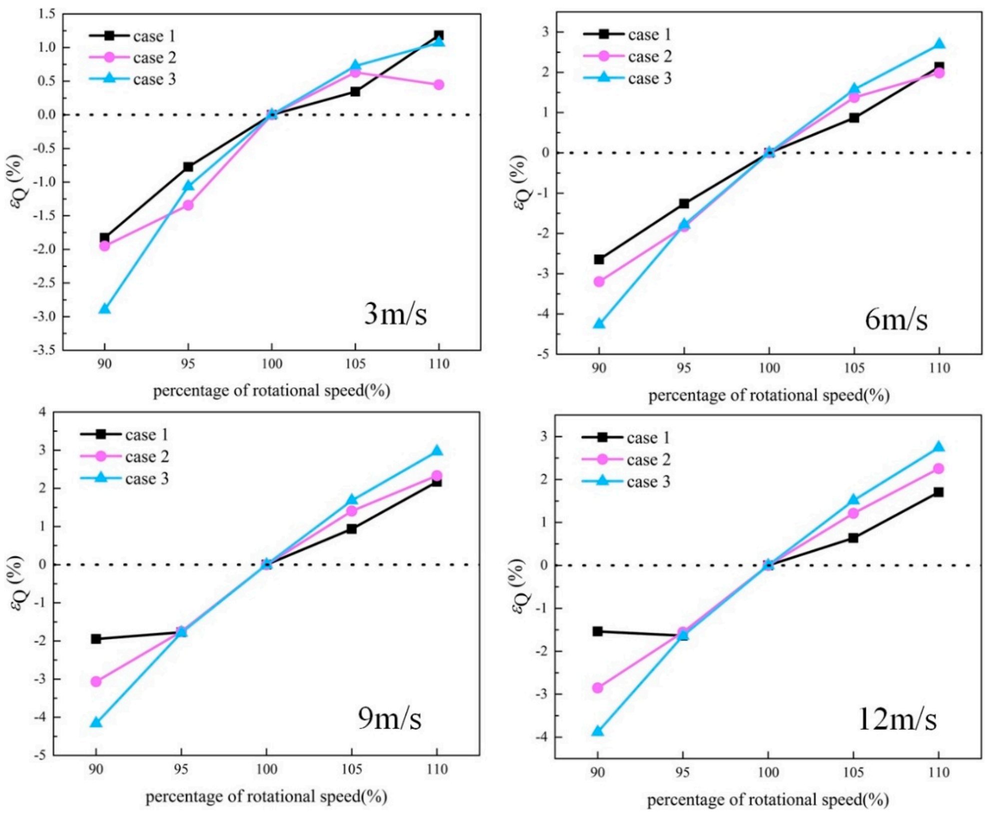

(**a**)

Figure 7. *Cont.*

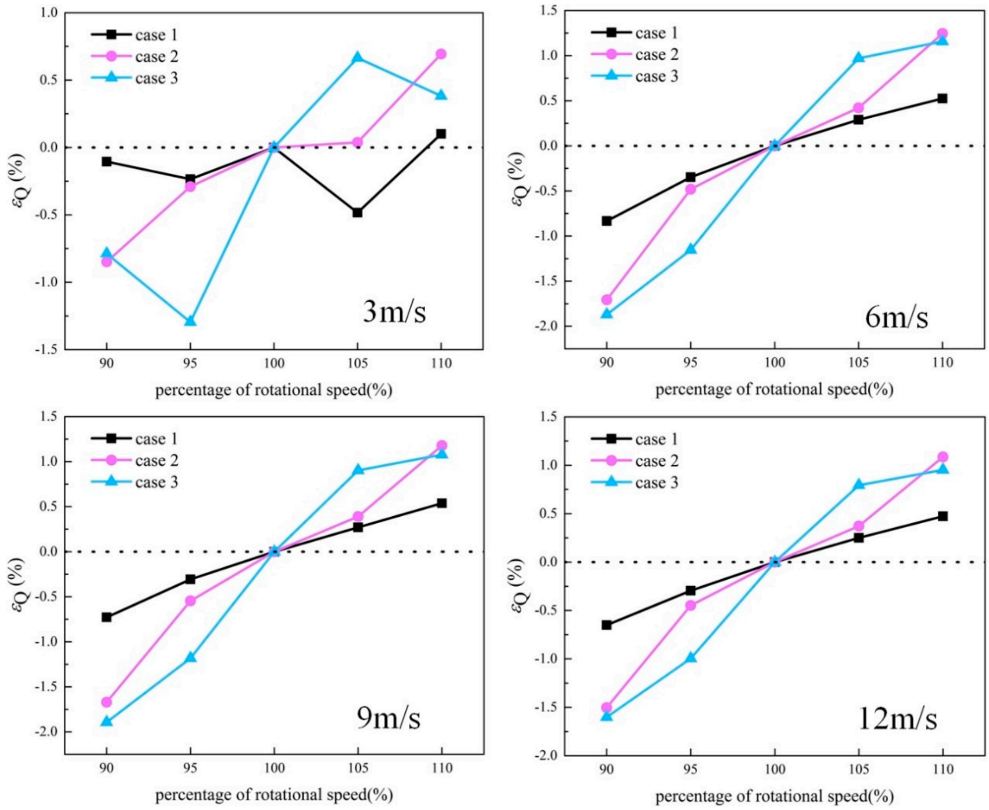

(**b**)

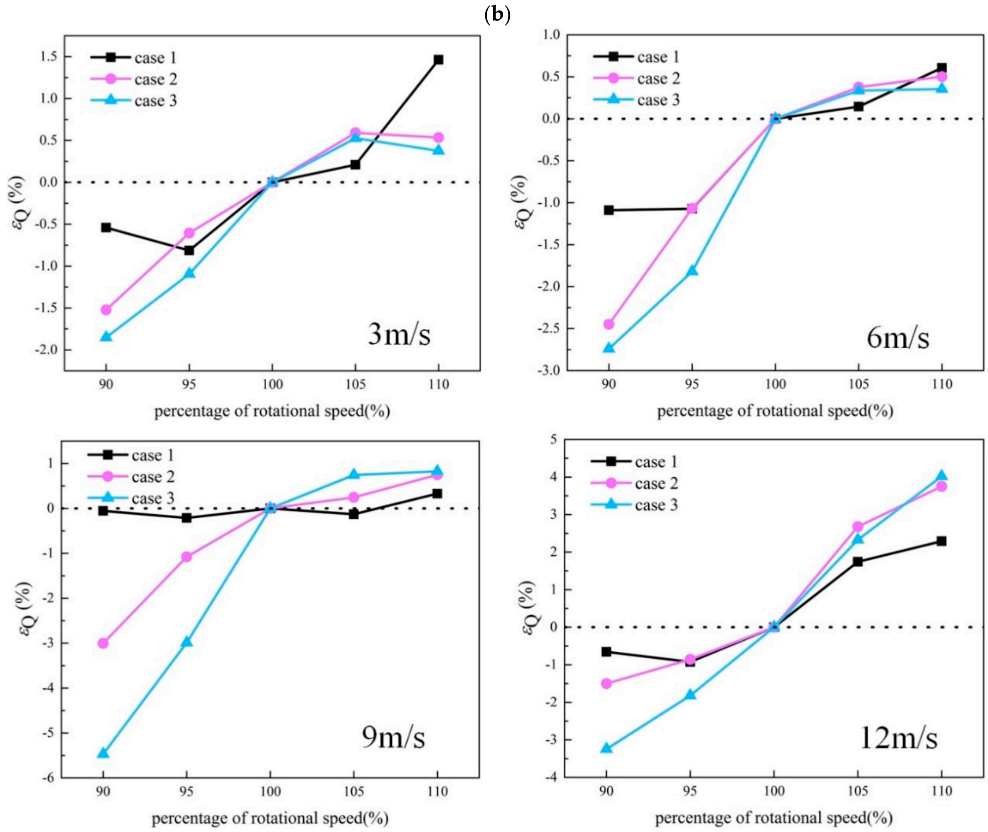

(**c**)

Figure 7. Improvement coefficient of heat rejection at various wind speeds. (**a**) In the wind direction of 90°; (**b**) in the wind direction of 0°; (**c**) in the wind direction of −90°.

Table 4. Mass flow rate and heat rejection of DDCS for various cases.

Wind Direction (°)	Wind Speed (m/s)	Percentage of Rotational Speed (%)	Case 1 Mass Flow Rate (kg/s)	Case 1 Heat Rejection (kW)	Case 2 Mass Flow Rate (kg/s)	Case 2 Heat Rejection (kW)	Case 3 Mass Flow Rate (kg/s)	Case 3 Heat Rejection (kW)
90	3	90	68,879	1,549,763	69,068	1,547,833	67,879	1,532,872
		95	69,711	1,566,394	69,246	1,557,416	69,612	1,561,803
		100	70,223	1,578,621	70,223	1,578,621	70,223	1,578,621
		105	70,288	1,584,041	70,672	1,588,579	70,828	1,590,086
		110	71,055	1,597,264	70,582	1,585,677	71,051	1,595,535
	6	90	61,487	1,417,979	61,491	1,409,946	60,398	1,394,444
		95	62,401	1,438,168	61,903	1,429,842	62,048	1,430,510
		100	62,941	1,456,545	62,941	1,456,545	62,941	1,456,545
		105	63,204	1,469,182	63,660	1,476,573	63,836	1,479,511
		110	64,065	1,487,630	63,877	1,485,461	64,473	1,495,690
	9	90	57,332	1,334,881	57,064	1,319,639	56,098	1,304,733
		95	57,553	1,337,247	57,437	1,337,495	57,545	1,337,105
		100	58,282	1,361,404	58,282	1,361,404	58,282	1,361,404
		105	58,455	1,374,118	58,834	1,380,497	59,077	1,384,267
		110	59,033	1,390,949	59,076	1,393,135	59,614	1,401,737
	12	90	55,345	1,293,718	55,133	1,276,424	54,276	1,262,936
		95	55,539	1,292,422	55,440	1,293,513	55,539	1,292,397
		100	56,146	1,313,930	56,146	1,313,930	56,146	1,313,930
		105	56,237	1,322,292	56,607	1,329,848	56,829	1,333,781
		110	56,722	1,336,313	56,827	1,343,527	57,348	1,349,968
0	3	90	72,721	1,621,333	71,839	1,609,264	72,007	1,610,250
		95	72,445	1,619,217	72,493	1,618,320	71,333	1,602,000
		100	72,623	1,623,033	72,623	1,623,033	72,623	1,623,033
		105	72,050	1,615,187	72,527	1,623,643	73,174	1,633,818
		110	72,564	1,624,674	73,141	1,634,291	72,726	1,629,238
	6	90	65,325	1,469,493	64,559	1,456,552	64,563	1,454,133
		95	65,523	1,476,696	65,499	1,474,718	64,801	1,464,737
		100	65,607	1,481,841	65,607	1,481,841	65,607	1,481,841
		105	65,678	1,486,122	65,707	1,488,071	66,271	1,496,227
		110	65,719	1,489,618	66,327	1,500,288	66,083	1,498,996
	9	90	59,717	1,372,035	58,987	1,359,010	58,935	1,355,934
		95	59,850	1,377,865	59,757	1,374,559	59,139	1,365,766
		100	59,883	1,382,105	59,883	1,382,105	59,883	1,382,105
		105	59,898	1,385,840	59,912	1,387,501	60,400	1,394,581
		110	59,913	1,389,540	60,407	1,398,398	60,195	1,397,001
	12	90	54,840	1,299,516	54,289	1,288,354	54,304	1,287,079
		95	54,961	1,304,162	54,943	1,302,169	54,457	1,295,007
		100	55,019	1,308,029	55,019	1,308,029	55,019	1,308,029
		105	55,038	1,311,296	55,051	1,312,888	55,432	1,318,416
		110	55,039	1,314,213	55,461	1,322,241	55,252	1,320,479
−90	3	90	60,863	1,374,528	61,100	1,360,978	60,335	1,356,419
		95	61,087	1,370,758	61,274	1,373,643	60,938	1,366,882
		100	61,451	1,382,008	61,451	1,382,008	61,451	1,382,008
		105	61,852	1,384,903	62,373	1,390,173	62,231	1,389,286
		110	62,931	1,402,216	62,174	1,389,393	62,038	1,387,204
	6	90	54,593	1,265,818	54,149	1,248,420	53,725	1,244,682
		95	54,888	1,266,043	54,880	1,266,096	54,181	1,256,483
		100	55,662	1,279,765	55,662	1,279,765	55,662	1,279,765
		105	55,986	1,281,610	56,269	1,284,576	56,278	1,284,057
		110	56,641	1,287,518	56,353	1,286,188	56,313	1,284,294
	9	90	50,326	1,165,777	48,410	1,131,406	47,386	1,102,634
		95	49,919	1,163,944	49,538	1,153,851	48,689	1,131,573
		100	50,187	1,166,434	50,187	1,166,434	50,187	1,166,434
		105	50,554	1,164,928	50,991	1,169,293	51,023	1,175,106
		110	51,118	1,170,260	51,046	1,175,176	51,103	1,176,050
	12	90	45,017	1,065,833	45,157	1,056,768	44,469	1,038,037
		95	45,440	1,062,964	45,377	1,063,689	44,739	1,053,349
		100	45,764	1,072,874	45,764	1,072,874	45,764	1,072,874
		105	46,606	1,091,565	47,054	1,101,590	46,886	1,097,847
		110	46,943	1,097,450	47,470	1,113,100	47,742	1,116,004

3.4. Turbine Back Pressure

The turbine back pressure is related to the temperature of the exhaust steam. The turbine back pressures for the optimal cases at different wind speeds in various wind directions can be calculated by the following formula without considering the steam pressure loss from the turbine to the condenser [35].

$$p_B = 0.00981\left(\frac{t_s + 100}{57.66}\right)^{7.46}, \tag{18}$$

As shown in Figure 8, the turbine back pressure in the wind direction of 90° is very close to that in the wind direction of 0°, while it is much higher in the wind direction of −90°. The back pressures in the wind directions of 90° and 0° increase almost linearly while it changes dramatically in the wind direction of −90° with the wind speed. The differences between the optimal cases and original cases are always small in the wind direction of 0° and reach the largest value of 0.53 kPa at the wind speed of 9 m/s. In the wind direction of 90°, the back pressure drop is slightly larger than the former and the largest back pressure drop is 1.34 kPa at the wind speed of 12 m/s. In the wind direction of −90°, the back pressure drop is not significant at low wind speeds, but increases sharply to 2.77 kPa when the wind speed reaches 12 m/s.

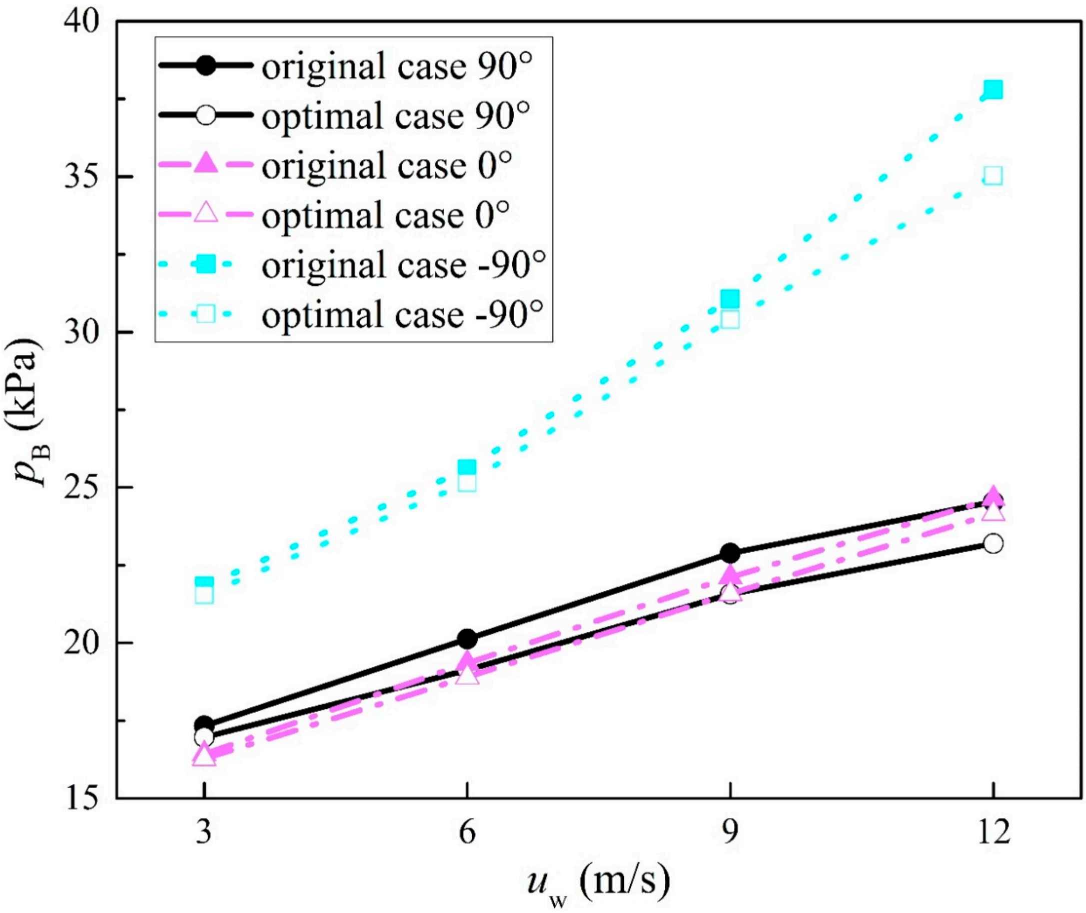

Figure 8. Turbine back pressures of optimal cases and original cases.

4. Conclusions

The ambient wind plays an unfavorable role in the cooling capacity of DDCS. By adjusting the rotational speeds of the fans in different blocks, the thermo-flow performance of DDCS under various ambient conditions is studied. The main results can be concluded as follows.

(1) The inlet air temperature of upwind fans significantly reduced when increasing the rotational speed of the windward fans. The changes in the rotational speed of the leeward fans have little effects on the inlet air temperature. The improvements for 110-case 1 are the most conspicuous in all of the wind directions;

(2) Generally speaking, increasing the rotational speeds of upwind fans is beneficial to the air flow rates under various wind conditions;
(3) The optimal strategies under different meteorological conditions can be obtained from the comparison of heat rejections. In the wind directions of 90° and −90°, the optimal strategies are 110-case 1 and 110-case 3 at the low and high wind speeds, respectively. In the wind direction of 0° however, 110-case 2 always performs best whatever the wind speed is;
(4) The turbine back pressures of the optimal strategies have improved when comparing with the original cases. The biggest drop in the turbine back pressure is 2.77 kPa in the wind direction of −90° at the wind speed of 12 m/s.

As a conclusion, it is recommended to adopt suitable operating strategies of axial flow fans according to environmental conditions for improving the cooling performance of DDCS.

Author Contributions: Conceptualization, W.H.; methodology, W.H.; software, W.H. and L.C. and W.W.; validation, W.H., L.C. and W.W.; formal analysis, W.H.; investigation, W.H.; resources, W.H.; data curation, W.H.; writing—original draft preparation, W.H.; writing—review and editing, L.Y.; visualization, L.Y.; supervision, L.Y.; project administration, L.Y. and X.D.; funding acquisition, L.Y. and X.D. All authors have read and agreed to the published version of the manuscript.

Funding: This research was funded by the National Natural Science Foundation of China (Grant No. 51776067, No. 51821004) and the Fundamental Research Funds for the Central Universities (Grant No. 2018QN036).

Conflicts of Interest: The authors declare no conflict of interest.

Nomenclature

c	number of windward adjusted fans
f_{n}	polynomial coefficient of the pressure drop for the fan
g_{n}	polynomial coefficient for the tangential velocity
h	convection heat transfer coefficient (W/m^2/K)
h'	empirical convection heat transfer coefficient (W/m^2/K)
h_{n}	polynomial coefficient for convection heat transfer coefficient
H	height above the ground (m)
k_{L}	pressure loss coefficient
L	thickness of the finned tube bundles (m)
n	rotational speed of fan
N	number
p	pressure (Pa)
P	shaft power
q	heat flux (W/m^2)
Q	heat transfer rate (kW)
r	the distance to the fan center
r_{n}	polynomial factor for pressure loss coefficient
S	source term
S'	additional source term
t	temperature (K)
u	velocity (m/s)
x	the percentage of actual rotational speed to rated speed
Greek symbols	
Γ	diffusion coefficient (m^2/s)
ρ	density (kg/m^3)
φ	dependent variable
ε	improvement coefficient of heat rejection
Subscripts	
0	original
2	outlet
a	air

B	back
e	energy
f	face velocity
j	direction
m	momentum
s	steam
v	volume
w	wind
z	z axis
θ	peripheral direction

References

1. Tawney, R.; Khan, Z.; Zachary, J. Economic and performance evaluation of heat sink options in combined cycle applications. *J. Eng. Gas Turbines Power.* **2005**, *127*, 397–403. [CrossRef]
2. Owen, M.; Kröger, D.G. A numerical investigation of vapor flow in large air-cooled condensers. *Appl. Therm. Eng.* **2017**, *127*, 157–164. [CrossRef]
3. Yang, L.J.; Du, X.Z.; Yang, Y.P. Space characteristics of the thermal performance for air-cooled condensers at ambient winds. *Int. J. Heat Mass Tran.* **2011**, *54*, 3109–3119. [CrossRef]
4. Yang, L.J.; Du, X.Z.; Yang, Y.P. Wind effect on the thermo-flow performances and its decay characteristics for air-cooled condensers in a power plant. *Int. J. Therm. Sci.* **2012**, *53*, 175–187. [CrossRef]
5. Rooyen, J.A.V.; Kröger, D.G. Performance trends of an air-cooled steam condenser under windy conditions. *J. Eng. Gas Turbines Power.* **2008**, *130*, 277–285. [CrossRef]
6. Wang, Q.W.; Zhang, D.J.; Zeng, M.; Lin, M.; Tang, L.H. CFD simulation on a thermal power plant with air-cooled heat exchanger system in north China. *Eng. Comput.* **2008**, *25*, 342–365. [CrossRef]
7. Liu, P.; Duan, H.; Zhao, W. Numerical investigation of hot air recirculation of air-cooled condensers at a large power plant. *Appl. Therm. Eng.* **2009**, *29*, 1927–1934. [CrossRef]
8. Gu, Z.; Li, H.; Zhang, W.; Li, Y.; Peng, J. Wind tunnel simulation on re-circulation of air-cooled condensers of a power plant. *J. Wind Eng. Ind. Aerod.* **2005**, *93*, 509–520. [CrossRef]
9. Gu, Z.; Chen, X.; Lubitz, W.; Li, Y.; Luo, W. Wind tunnel simulation of exhaust recirculation in an air-cooling system at a large power plant. *Int. J. Therm. Sci.* **2007**, *46*, 308–317. [CrossRef]
10. Gao, X.F.; Zhang, C.W.; Wei, J.J.; Yu, B. Performance prediction of an improved air-cooled steam condenser with deflector under strong wind. *Appl. Therm. Eng.* **2010**, *30*, 2663–2669. [CrossRef]
11. Yang, L.; Du, X.; Yang, Y. Measures against the adverse impact of natural wind on air-cooled condensers in power plant. *Sci. China Technol. Sci.* **2010**, *53*, 1320–1327. [CrossRef]
12. Zhang, X.; Wu, T. Effects of diffuser orifice plate on the performance of air-cooled steam condenser. *Appl. Therm. Eng.* **2016**, *98*, 179–188. [CrossRef]
13. Huang, X.; Chen, L.; Kong, Y.; Yang, L.; Du, X. Effects of geometric structures of air deflectors on thermo-flow performances of air-cooled condenser. *Int. J. Heat Mass Tran.* **2018**, *118*, 1022–1039. [CrossRef]
14. Xiao, L.; Ge, Z.; Yang, L.; Du, X. Numerical study on performance improvement of air-cooled condenser by water spray cooling. *Int. J. Heat Mass Tran.* **2018**, *125*, 1028–1042. [CrossRef]
15. Huang, X.; Zhang, X. Field test and research on heat-transfer performance of plate air-cooled condenser. *Procedia Environ. Sci.* **2011**, *10*, 1148–1153. [CrossRef]
16. Jin, R.; Yang, X.; Yang, L.; Du, X.; Yang, Y. Square array of air-cooled condensers to improve thermo-flow performances under windy conditions. *Int. J. Heat Mass Tran.* **2018**, *127*, 717–729. [CrossRef]
17. Kong, Y.; Wang, W.; Huang, X.; Yang, L.; Du, X. Annularly arranged air-cooled condenser to improve cooling efficiency of natural draft direct dry cooling system. *Int. J. Heat Mass Tran.* **2018**, *118*, 587–601. [CrossRef]
18. Yang, L.J.; Wang, M.H.; Du, X.Z.; Yang, Y.P. Trapezoidal array of air-cooled condensers to restrain the adverse impacts of ambient winds in a power plant. *Appl. Energ* **2012**, *99*, 402–413. [CrossRef]
19. Duvenhage, K.; Kröger, D.G. The influence of wind on the performance of forced draught air-cooled heat exchangers. *J. Wind Eng. Ind. Aerodyn.* **1996**, *62*, 259–277. [CrossRef]
20. Duvenhage, K.; Vermeulen, J.A.; Meyer, C.J.; Kröger, D.G. Flow distortions at the fan inlet of forced-draught air-cooled heat exchangers. *Appl. Therm. Eng.* **1996**, *16*, 741–752. [CrossRef]

21. Meyer, C.J. Numerical investigation of the effect of inlet flow distortions on forced draught air-cooled heat exchanger performance. *Appl. Therm. Eng.* **2005**, *25*, 1634–1649. [CrossRef]
22. Hotchkiss, P.J.; Meyer, C.J.; von Backström, T.W. Numerical investigation into the effect of cross-flow on the performance of axial flow fans in forced draught air-cooled heat exchangers. *Appl. Therm. Eng.* **2006**, *26*, 200–208. [CrossRef]
23. He, W.F.; Zhang, X.K.; Han, D.; Gao, L. Sensitivity analysis from the blade angle regulation of the forced draught fans in an air-cooled steam condenser. *Appl. Therm. Eng.* **2017**, *123*, 810–819. [CrossRef]
24. He, W.; Dai, Y.; Han, D.; Yue, C.; Pu, W. Influence from the rotating speed of the windward axial fans on the performance of an air-cooled power plant. *Appl. Therm. Eng.* **2014**, *65*, 14–23. [CrossRef]
25. He, W.F.; Chen, J.J.; Han, D.; Wen, T.; Luo, L.T.; Li, R.Y.; Zhong, W.C. Numerical analysis from the rotational speed regulation within the fan array on the performance of an air-cooled steam condenser. *Appl. Therm. Eng.* **2019**, *153*, 352–360. [CrossRef]
26. Yang, T.; Wang, W.; Zeng, D.; Liu, J.; Cui, C. Closed-loop optimization control on fan speed of air-cooled steam condenser units for energy saving and rapid load regulation. *Energy* **2017**, *135*, 394–404. [CrossRef]
27. Jin, R.; Yang, X.; Yang, L.; Du, X.; Yang, Y. Thermo-flow performances of air-cooled condenser cell with oblique finned tube bundles. *Int. J. Therm. Sci.* **2019**, *135*, 478–492. [CrossRef]
28. Kong, Y.; Wang, W.; Yang, L.; Du, X. Energy efficient strategies for anti-freezing of air-cooled heat exchanger. *Appl. Energ* **2020**, *261*, 114468. [CrossRef]
29. Dukhan, N.; Bagcı, O.; Ozdemir, M. Metal foam yhdrodynamics: Flow regimes from pre-Darcy to turbulent. *Int. J. Heat Mass Tran.* **2014**, *77*, 114–123. [CrossRef]
30. Errasti, I.; Fernández, U.; Martinez-Filgueira, P.; Blanco, J.M. Source term modelling of vane-type vortex generators under adverse pressure gradient in OpenFOAM. *Energies* **2019**, *12*, 605. [CrossRef]
31. ANSYS Inc. *Fluent User's Guide*; ANSYS Inc.: Canonsburg, PA, USA, 2012.
32. Chen, L.; Yang, L.; Du, X.; Yang, Y. A novel layout of air-cooled condensers to improve thermo-flow performances. *Appl. Energ* **2016**, *165*, 244–259. [CrossRef]
33. Chen, L.; Sun, Y.; Yang, L.; Du, X.; Yang, Y. Rotational speed adjustment of axial flow fans to maximize net power output for direct dry cooling power generating units. *Heat Transf.-Asian Res.* **2020**, *49*, 356–382. [CrossRef]
34. Kong, Y.; Wang, W.; Huang, X.; Yang, L.; Du, X.; Yang, Y. Circularly arranged air-cooled condensers to restrain adverse wind effects. *Appl. Therm. Eng.* **2017**, *124*, 202–223. [CrossRef]
35. Yang, L.J.; Wu, X.P.; Du, X.Z.; Yang, Y.P. Dimensional characteristics of wind effects on the performance of indirect dry cooling system with vertically arranged heat exchanger bundles. *Int. J. Heat Mass Tran.* **2013**, *67*, 853–866. [CrossRef]